Frustrated pretransitional phenomena in aperiodic composites

C. Mariette, Ilya Frantsuzov, Bo Wang, L. Guérin, P. Rabiller, Mark D. Hollingsworth, and B. Toudic

Frustrated pretransitional phenomena in aperiodic composites

C. Mariette,[1a] Ilya Frantsuzov,[2] Bo Wang,[2] L. Guérin,[1] P. Rabiller,[1] Mark D. Hollingsworth,[2a] B. Toudic[1]

[1] *Institut de Physique de Rennes, UMR UR1-CNRS 6251, Université de Rennes 1, 35042 Rennes, France*

[2] *Department of Chemistry, 213 CBC Building, Kansas State University, Manhattan, Kansas 66506-0401, U.S.A.*

[a]Authors to whom correspondence should be addressed: celine.mariette@univ-rennes1.fr; mdholl@ksu.edu

Abstract

This Letter reports on symmetry breaking in the aperiodic inclusion compound *n*-octadecane/urea and its isotopomer *n*-octadecane/urea-d$_4$. The high-symmetry phase is described by a hexagonal rank four superspace group. Pretransitional phenomena in this crystallographic superspace reveal competing short-range ordering phenomena within the high-symmetry phase. Very high-resolution diffraction data shows that critical scattering appears at inequivalent points within the four-dimensional Brillouin zone, although the first phase transition at T_{c1} near 158 K implies the condensation at only one of those points. The resulting superspace group remains of dimension four. Two other phase transitions are reported at $T_{c2} = 152.8(4)$ K and $T_{c3} = 109(4)$ K in *n*-octadecane/urea-d$_4$. The two low-symmetry phases that arise are described by rank five superspace groups.

I. INTRODUCTION

Phase transitions and critical pretransitional fluctuations have been studied extensively for more than fifty years [1, 2]. Group/sub-group relations describe the observed symmetry lowering. Evaluation of the long-range ordering in different phases using diffraction techniques provides information on the actual symmetry of each phase, whereas diffuse scattering associated with short-range order in the precursor phases gives essential

information on the interactions involved. In certain cases, competition between different types of long-range ordering exists in the crystal, but a phase transition gives rise to only one of them. A notable example is the molecule of fullerene, which illustrates such a feature in three-dimensional crystallographic space [3-5]. With aperiodic materials, standard crystallography must be generalized to higher dimensional spaces, where translational symmetry is recovered. We have already reported symmetry breaking in higher-dimensional spaces by defining and analyzing both the mean order parameter and its spatial fluctuations (pretransitional short-range order) [6]. Here we report the existence of a competition between two different types of long-range ordering within a four-dimensional superspace group. When compared with the 3D to 3D phase transition in the fullerene crystal, an additional complexity is that these two competing phases do not have the same dimensionality in crystallographic superspace.

Here, we will focus on an organic aperiodic composite. Aperiodic composites arise from the imbrication of two or more incommensurate substructures in which interactions of the components give rise to mutual incommensurate modulations [7-10]. For uniaxial composites, such as host-guest systems, there is a single incommensurate direction (c), and the reciprocal image of a four-dimensional crystal is characterized by the superspace description

$$\mathbf{Q}_{hklm} = h \cdot \boldsymbol{a}^* + k \cdot \boldsymbol{b}^* + l \cdot \boldsymbol{c_h}^* + m \cdot \boldsymbol{c_g}^*$$

in which $\boldsymbol{a}^*$ and $\boldsymbol{b}^*$ are the conventional reciprocal unit cell vectors, while $\boldsymbol{c_h}^*$ and $\boldsymbol{c_g}^*$ are those of the host and guest, respectively, along the aperiodic direction. In the case of a five-dimensional crystal, there is a supplementary reciprocal unit cell vector along the aperiodic direction, $\boldsymbol{c_m}^*$, and the basis is

$$\mathbf{Q}_{hklmn} = h \cdot \mathbf{a}^* + k \cdot \mathbf{b}^* + l \cdot \boldsymbol{c_h}^* + m \cdot \boldsymbol{c_g}^* + n \cdot \boldsymbol{c_m}^*.$$

The real-space repeat lengths of the host, guest, and supplementary modulation are $c_h = 1/\boldsymbol{c_h}^*$, $c_g = 1/\boldsymbol{c_g}^*$, and $c_m = 1/\boldsymbol{c_m}^*$, respectively, with the latter two usually being defined in terms of the host via irrational misfit parameters $\gamma = c_h/c_g$ and $\delta = c_h/c_m$. A convenient labeling for the different types of Bragg peaks is that ($h\ k\ 0\ 0\ 0$), ($h\ k\ l\ 0\ 0$), ($h\ k\ 0\ m\ n$), and ($h\ k\ l\ m\ n$), with l and m different from zero, are the common, host, guest, and satellite Bragg peaks, respectively, with the recognition that both substructures contribute to each kind of Bragg peak due to the aforementioned interactions.. Throughout this paper, Miller planes indexed

with hexagonal and orthorhombic cells are denoted with subscripts "h" and "o", respectively; for example $(h\ k\ l\ m\ n)_o$. In the orthorhombic basis, reflections with $h + k$ = even are referred to as 'structure' peaks, and those with $h + k$ = odd are referred to as 'superstructure' peaks.
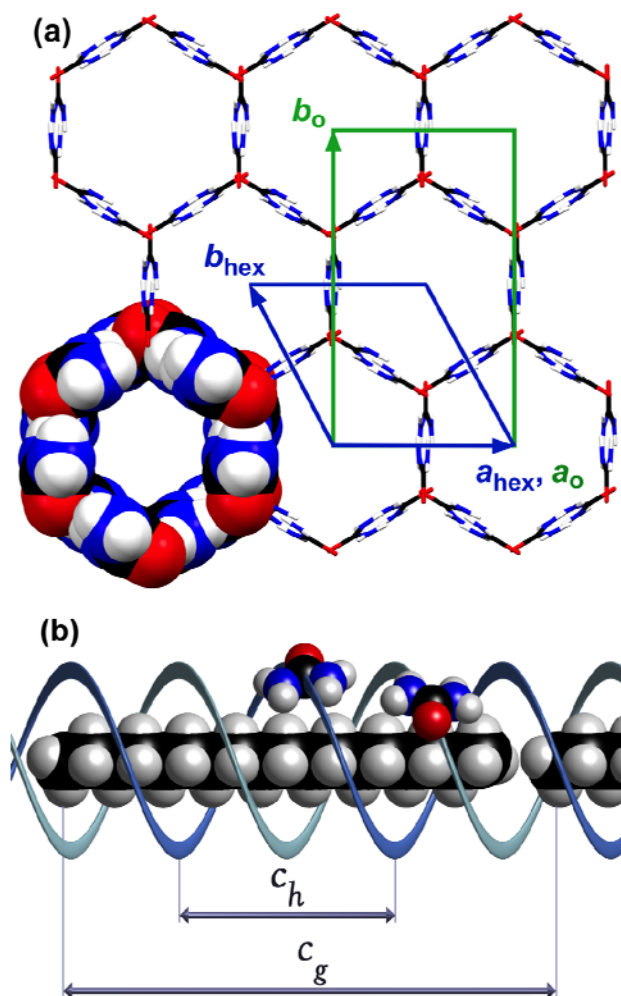

FIG. 1. (Color online) (a) Channel axis view of the host structure of a urea inclusion compound, showing the unit cell axes for the high temperature hexagonal form (blue) and the low temperature orthorhombic forms (green). Coordinates are from reference 11. With an undistorted (orthohexagonal) channel, $b_o = \sqrt{3}a_o$. Space-filling models (lower left) show that the van der Waals diameter of the channel is somewhat larger than the van der Waals envelope of a linear hydrocarbon. (b) Schematic structure of n-octadecane/urea viewed perpendicular to the channel axis, showing the definitions of c_h and c_g.

Prototypical examples of such aperiodic composites are n-alkane/urea inclusion compounds [12-16]. In these supramolecular systems urea molecules form a helical,

hydrogen-bonded network of parallel, hexagonal channels with internal diameters of 5.5-5.8 Å (Figure 1)[17]. A large body of work has been dedicated to the phase transitions in this prototype family [18-33], revealing recently a rich sequence of phases in high-dimensional crystallographic spaces [6, 11, 18, 19, 32, 33]. Previously, we reported original behavior of the critical phenomena leading to a phase transition with an increase of the dimensionality of the crystallographic superspace from four to five [6, 19]. Here, we report the existence of frustrated pretransitional phenomena in n-octadecane/urea and its isotopomer n-octadecane/urea-d_4.

II. EXPERIMENTAL DETAILS

For the pretransitional diffuse scattering studies, high-flux and high-resolution measurements were performed on beamline 14-BM-C at the APS synchrotron, with a fixed wavelength of $\lambda = 0.97870$ Å. Measurements were done with a single ϕ-axis rotation goniometer and a cooled ADSC Quantum 315 CCD detector with very low noise, allowing measurements of low-intensity diffuse scattering. For some of these measurements, in order to limit the exposure and thus prevent crystal damage, a very small part of reciprocal space was probed using 15° ϕ rotations in 0.8° steps around the zone of interest. Subsequently, the diffraction planes where reconstructed using CrysAlisPro software from Agilent Technologies. Remaining measurements were made using 60° ϕ rotations of crystals aligned with their c axes along the ϕ axis of the goniostat, as noted in figure captions. The detector was placed as far as 800 mm from the sample, in order to obtain the highest possible spatial resolution.

In all cases, the crystals were cooled with flowing nitrogen stream from an Oxford Cryostream from Oxford Cryosystems Ltd. Differential scanning calorimetry measurements were performed using a DSC Q2000 from TA Instruments and a Perkin Elmer Pyris 1 DSC. Crystals of n-octadecane/urea were grown by slowly cooling a solution containing n-octadecane (Fluka, 99.8%, 311 mg), urea (Sigma Ultra, 353 mg), methanol (10.0 mL), and 2-methyl-2-propanol (9.0 mL) containing 1% (v/v) water from 51 ºC to room temperature. Crystals of n-octadecane/urea-d_4 were grown by slowly cooling a solution of n-octadecane (Fluka, 99.8%, 361 mg), urea-d_4 (Aldrich, 98%D, 995 mg), methanol-d_1 (Aldrich, 99.5%D, 10.0 mL), and 2-methyl-2-propanol-d_1 (Aldrich, 99%D, 2.0 mL) from 45 ºC to 4 ºC. Solution phase ^{1}H NMR (400 MHz, DMF-d_7) of n-octadecane/urea-d_4 showed less than 0.7% methanol (relative to guest) and no detectable 2-methyl-2-propanol in the channels. No trace of either solvent was found in n-octadecane/urea (400 MHz, DMSO-d_6).

Measurements of reciprocal lattice spacings from *n*-octadecane/urea and *n*-octadecane/urea-d$_4$ were found to be the same within experimental uncertainty and are used interchangeably throughout this manuscript. Individual frames were analysed using WxDiff [34] and local scripts for MATLAB® [35]. Unless otherwise stated, errors are reported as standard errors of the mean. The term e.s.d. refers to the standard deviation of the sample. Error bars in graphs of peak intensities and misfit parameters are estimates and should not be treated as absolute errors.

III. RESULTS

At room temperature, crystals of *n*-octadecane/urea exhibit intermodulation of two substructures with common *a* and *b* unit cell parameters. This parent phase (Phase I) is described by the four-dimensional superspace group P6$_1$22(00γ) [15]. Figure 2 presents the temperature evolution of the heat flow as measured when cooling and heating the system at a rate of 10 K/min. Between 135 and 170 K, two events are observed, a rather weak one at T$_{c1}$ around 160 K, and another, much stronger one, at T$_{c2}$, around 154-155 K. In *n*-octadecane/urea-d$_4$, T$_{c2}$ was approximately 1.8 K lower than in *n*-octadecane/urea.
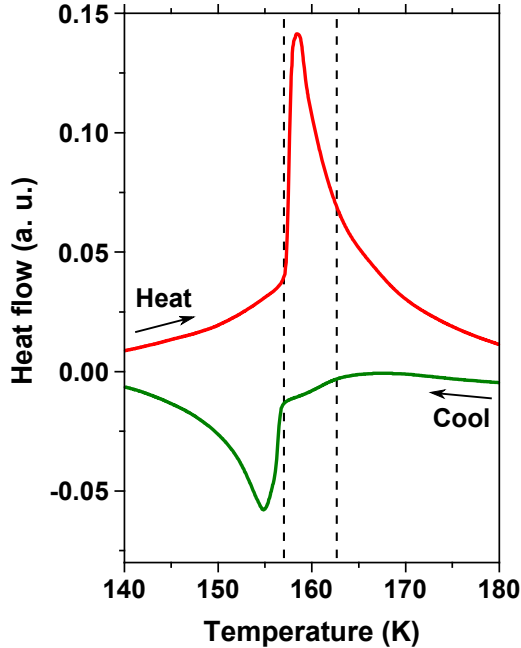
FIG. 2. (Color online) Differential scanning calorimetry trace of *n*-octadecane/urea with heating and cooling rates of 10 K/min (green cooling curve, red warming curve, endothermic up) showing the strong signature of the ferroelastic transition associated with the formation of Phase III. The dashed lines highlight the inflection points at the upper and lower ends of the

small exotherm associated with the formation of Phase II during cooling. Because it was so weak and occurred at such a low temperature, the transition at T_{c3} was not accessible to our calorimeters. Studies of an analogous transition in nonadecane/urea indicate that it is also very weak and is exothermic during cooling [36].

Figure 3 presents diffraction images measured at different temperatures corresponding to four different crystallographic phases (I-IV) that occur successively when cooling the crystal. At 163.1 K, the high-symmetry Phase I exhibits several combinatory Bragg peaks (h k l m)$_h$ with l and m different from zero, demonstrating intermodulation of this aperiodic crystal in this phase. The pretransitional streaks observed at this temperature condense into superstructure Bragg peaks at T_{c1}= 158.1(4) K, indicating the transition to an orthorhombic basis. At T_{c2} = 152.8(4) K and below, the orthorhombic unit cell becomes distorted from metric hexagonal symmetry, as shown in Fig. 4 for the unit cell parameters a and b. Such ferroelastic phase transitions were previously reported for many crystals in the n-alkane/urea family. A fit of the distortion of a_o and b_o to $A(T_c-T)^\beta$ gives a low critical exponent, $\beta \approx$ 0.186, indicating a weakly first-order phase transition. The differences between Phases II, III and IV demonstrate competing order parameters, and a detailed study of the critical phenomena is presented in the next section.

For n-octadecane/urea-d$_4$ at 100.3 K, the orthorhombic cell constants were a_o = 8.2572 (13) Å and b_o = 13.843(2) Å from 26 reflections, and c_h = 10.9580(9) Å from 50 reflections using a detector distance of 440 mm; as measured from the two (1 1 ±2 0 0)$_o$ peaks in the temperature range from 100.3 to 200 K, c_h increased linearly with a slope of 0.000204(4) Å/K.
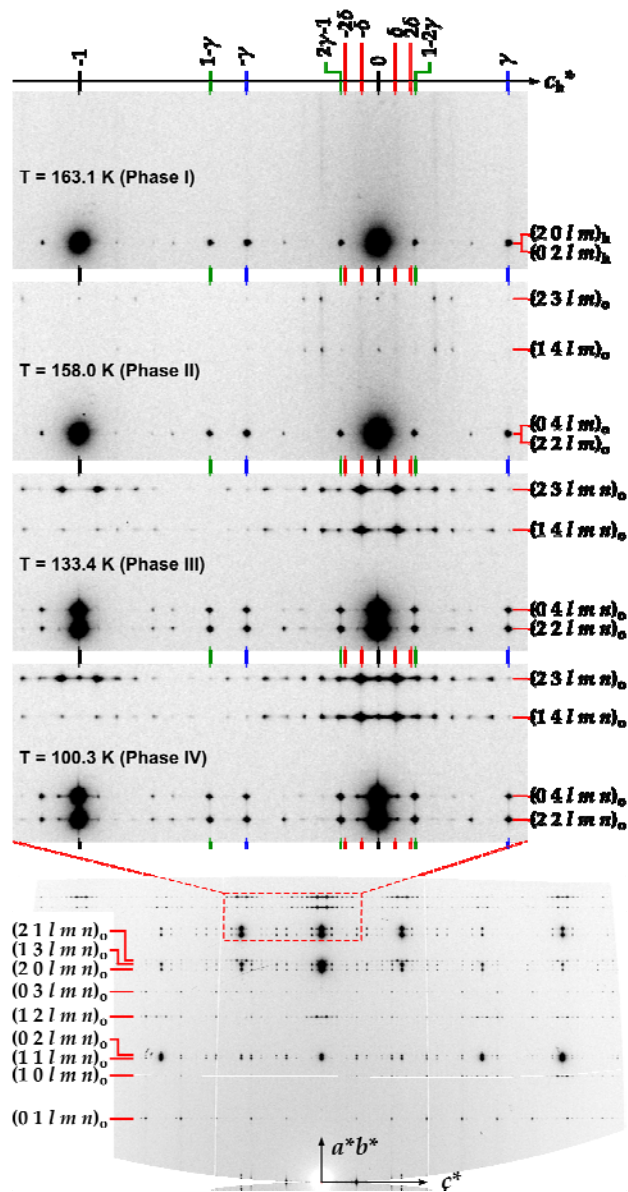
FIG. 3. (Color online) Sections of diffraction images of *n*-octadecane/urea-d$_4$ across a range of temperatures. The large frame section at the bottom was collected at 100.3 K. Measurements were made using 60° φ rotations about the crystal *c* axis at a detector distance of 440 mm (λ = 0.97870 Å) on beamline 14-BM-C at the APS.
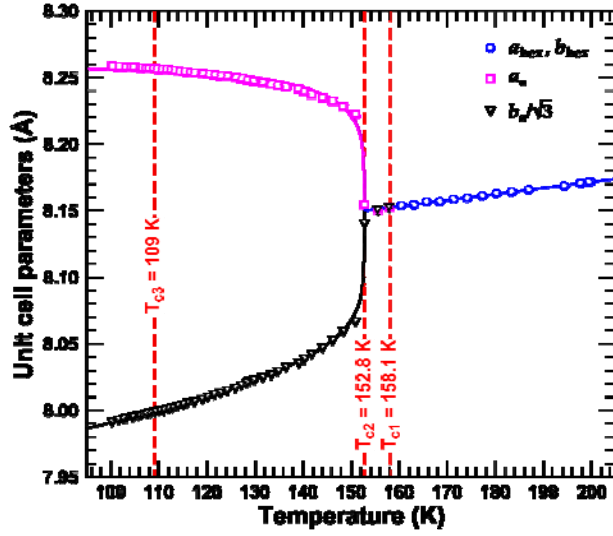
FIG. 4. (Color online) Temperature evolution of the unit cell parameters of n-octadecane/urea-d$_4$. For the hexagonal Phase I (blue circles), the cell parameters were measured from the positions of the $(\pm 2\ 0\ 0\ 0)_h$ peaks and fit to a straight line, giving: $(a_{hex}, b_{hex}) = 0.000458 \times T + 8.08$. For the orthorhombic Phases II to IV, the cell parameters a_o (pink squares) and b_o (black triangles) were measured from the position of the $(\pm 2\ 0\ 0\ 0\ 0)_o$ and $(0\ \pm 4\ 0\ 0\ 0)_o$ peaks, respectively. Note that below $T_{c1} = 158.1(4)$ K, the Laue symmetry changes from hexagonal to orthorhombic (as shown in Figures 3 and 7), but no ferroelastic distortion is observed. At T_{c2}, greater accuracy was achieved by using an average of all the $(h\ k\ 0\ 0\ 0)_o$ peaks. The values of b_o were divided by $\sqrt{3}$ to make them more comparable to the other cell parameters. Below $T_{c2} = 152.8(4)$ K, the orthorhombic cell exhibits a ferroelastic distortion. The unit cell parameters below T_{c2} were fit to $\pm A(T_{c2} - T)^{\beta} + (0.000458 \times T + 8.08)$. The critical exponent, β, was measured to be 0.199(5) and 0.173(4) for a_o and b_o, respectively. Measurements were made using 60° ϕ rotations about the crystal c axis at a detector distance of 440 mm on beamline 14-BM-C at the APS.

The misfit parameter, $\gamma = c_h/c_g$, representing the guest chain length relative to the urea host repeat was found to be the same in all four phases, for both n-octadecane/urea and n-octadecane/urea-d$_4$. It was measured to be $\gamma = 0.43776(2)$ for $(1\ 1\ l\ m\ n)_o$ of n-octadecane/urea-d$_4$, as shown in Fig. 5. The misfit parameter of the supplementary modulation, $\delta = c_h/c_m$, was also unchanged across phases III and IV, as shown in Fig. 6 for several superstructure layer lines of n-octadecane/urea-d$_4$. Note that the deviation of δ from the mean near $T_{c2} = 152.8(4)$ K is not consistent between layer lines and is attributed to increased uncertainties in the parameter fits of the weak pretransitional scattering rather than

to an actual change in δ. Since these measurements of δ were taken from the same set of frames, differences between the mean values for different layer lines must be due to systematic errors between different regions of the detector (which can be understood in terms of imperfect crystal and detector alignment) and are estimated to be of the order of 1/5 of a detector pixel width. With these systematic errors in mind, the mean values of the misfit parameters are estimated to be $\gamma = 0.4378(6)$ and $\delta = 0.0576(6)$ (e.s.d.). It is notable that $\gamma/\delta = 7.60(8)$ (e.s.d.), which, not being an integer, validates the use of a 5D description (since the long-range modulation wavelength is therefore not an integral number of guest repeat lengths).
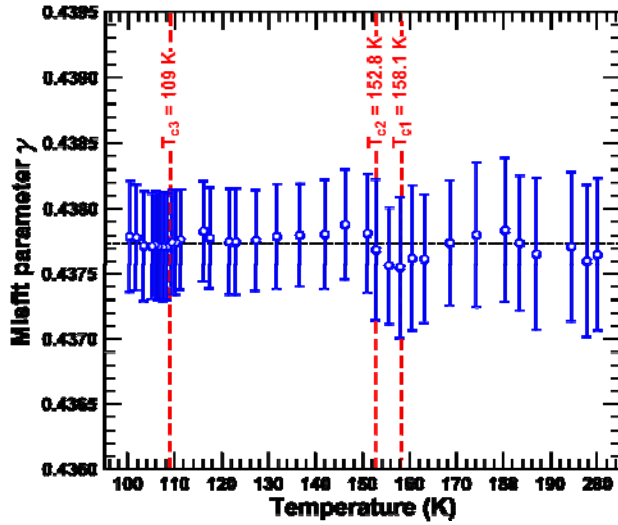

FIG. 5. (Color online) Temperature evolution of the misfit parameter γ of n-octadecane/urea-d_4. This was determined from simultaneous least-squares fits of all of the peaks in the $(1\ 1\ l\ m\ n)_o$ layer line from $Qc_h* = -0.16$ to 3.75. The horizontal dashed line is a least-squares fit to a constant misfit parameter that takes into account the uncertainty in each point, giving $\gamma = 0.43776(2)$. Measurements were made using 60° ϕ rotations about the crystal c axis at a detector distance of 440 mm on beamline 14-BM-C at the APS.
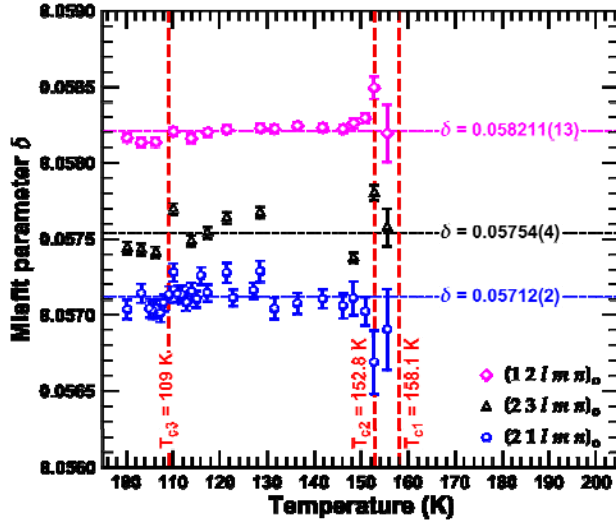
FIG. 6. (Color online) Temperature evolution of the supplementary misfit parameter δ of n-octadecane/urea-d$_4$. Measurements were made using 60° φ rotations about the crystal c axis at a detector distance of 440 mm on beamline 14-BM-C at the APS. Data at the same temperature were taken from the same frame at different positions in reciprocal space in a given Qc_h^* range (from 0.15 to 2.23 for (1 2 l m n)$_o$, and from -0.15 to 1.35 for (2 1 l m n)$_o$ and (2 3 l m n)$_o$). The misfit parameter was determined from simultaneous least-squares fits of all peaks in the respective Qc_h^* range, leading to the represented error bars. The precision of these fits is sufficient to show that the value of δ is constant as a function of temperature within a consistent set of measurements. The small differences between the mean values of δ for each layer line are due to slight misalignment of the detector and crystal rather than physical differences in the supplementary modulation wavelength. Averaging these values gives a single mean value of δ = 0.0576(6) (e.s.d.) for the crystal.

IV. COMPETING ORDER PARAMETERS

To demonstrate the signatures of each phase transition, Fig. 7 shows a region of the (1 2 l m n)$_o$ superstructure layer line around the common peak for a range of temperatures. Phase II is characterized by the transition from a hexagonal unit cell to an orthorhombic one due to partial alignment of guest molecules in neighboring channels, marked by the appearance of the (1 2 0 0 0)$_o$ common peak around T_{c1} = 158.1(4) K in Fig. 7b. At the second phase transition around T_{c2} = 152.8(4) K, the host (e.g., (2 3 -1 0)$_o$ – see Fig. 3) and common peaks in the superstructure layer lines diminish in intensity, while peaks associated with the supplementary modulation appear, with the latter indicating additional ordering of the guest molecules along the channel axis with a modulation wavelength of c_m = 190(3) Å.
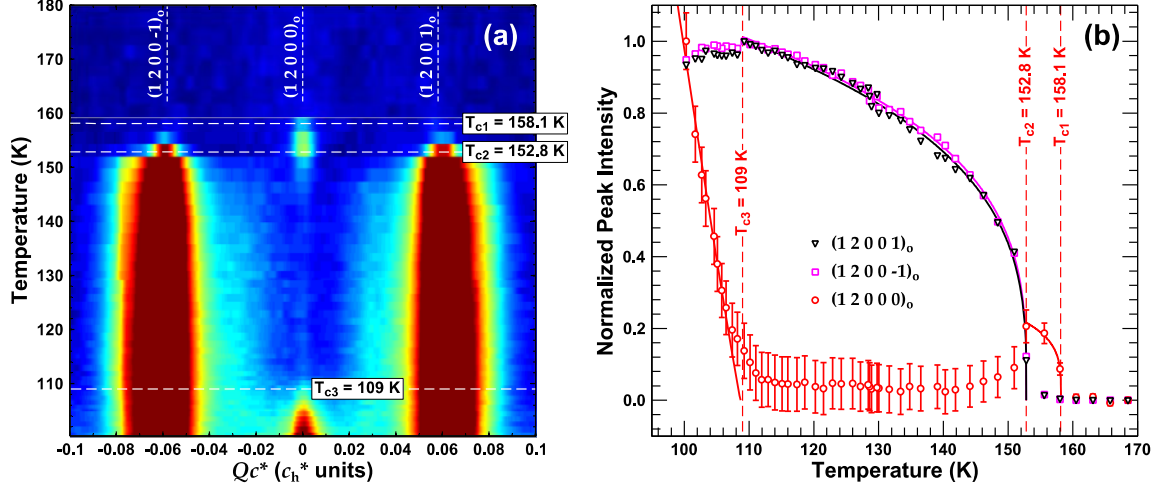
FIG. 7. (Color online) Temperature evolution of the $(1\ 2\ l\ m\ n)_o$ superstructure layer line of n-octadecane/urea-d_4 upon cooling. Measurements were made using 60° ϕ rotations about the crystal c axis at a detector distance of 440 mm on beamline 14-BM-C at the APS. (a) Evolution of peak intensities along c_h*, shown on a logarithmic color scale, with red being most intense. The boundaries between horizontal sections correspond to the mean temperature of those two frames. (b) Normalized peak intensities as a function of temperature, with solid lines fit to $A(T_c - T)^\beta$. The critical exponent, β, was measured to be 0.25(3) and 1.1(8) for $(1\ 2\ 0\ 0\ 0)_o$ at T_{c1} and T_{c3}, respectively; it was 0.305(7) for $(1\ 2\ 0\ 0\ 1)_o$ and 0.294(4) for $(1\ 2\ 0\ 0\ -1)_o$ at T_{c2}. In unlabeled n-octadecane/urea, T_{c2} is approximately 1.8 K higher.

Measurements of the diffuse scattering preceding the appearance of the common and supplementary modulation peaks were performed in order to characterize two different types of critical pretransitional phenomena at these temperatures. In the high-symmetry hexagonal notation, the respective critical wavevectors are $\mathbf{q}_{c1} = (0\ ½\ 0\ 0)_h$ and $\mathbf{q}_{c2} = (0\ ½\ \delta\ 0)_h$, as shown in Fig. 8. Analysis of the disc-shaped pretransitional diffuse X-ray scattering in the vicinity of $(2\ 3\ 0\ 0\ 0)_o$ and $(2\ 3\ 0\ 0\ 1)_o$ allows one to determine the ellipsoids associated with the correlation lengths $(\zeta_a, \zeta_b, \zeta_c)$; the principal axes of these ellipsoids lie along the directions $\mathbf{a}_o*$, $\mathbf{b}_o*$, and $\mathbf{c}_h*$ of the orthorhombic reciprocal cell [6].
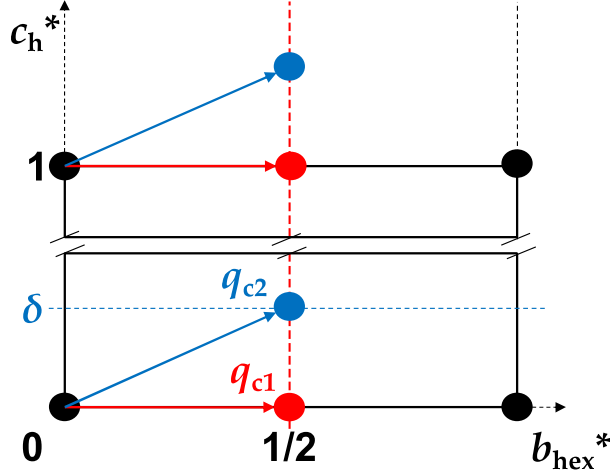
FIG. 8. (Color online) Schematic representation of a section of the high-symmetry hexagonal reciprocal space of the aperiodic, four-dimensional crystal of n-octadecane/urea in the superspace group (P6$_1$22(00γ)). The critical point associated with the wave vector q_{c1} = (0 ½ 0 0)$_h$ is shown in red, and that of the wave vector q_{c2} = (0 ½ δ 0)$_h$ is shown in blue. These would be (0 1 0 0)$_o$ and (0 1 0 0 1)$_o$, respectively, in their four- and five-dimensional orthorhombic bases.
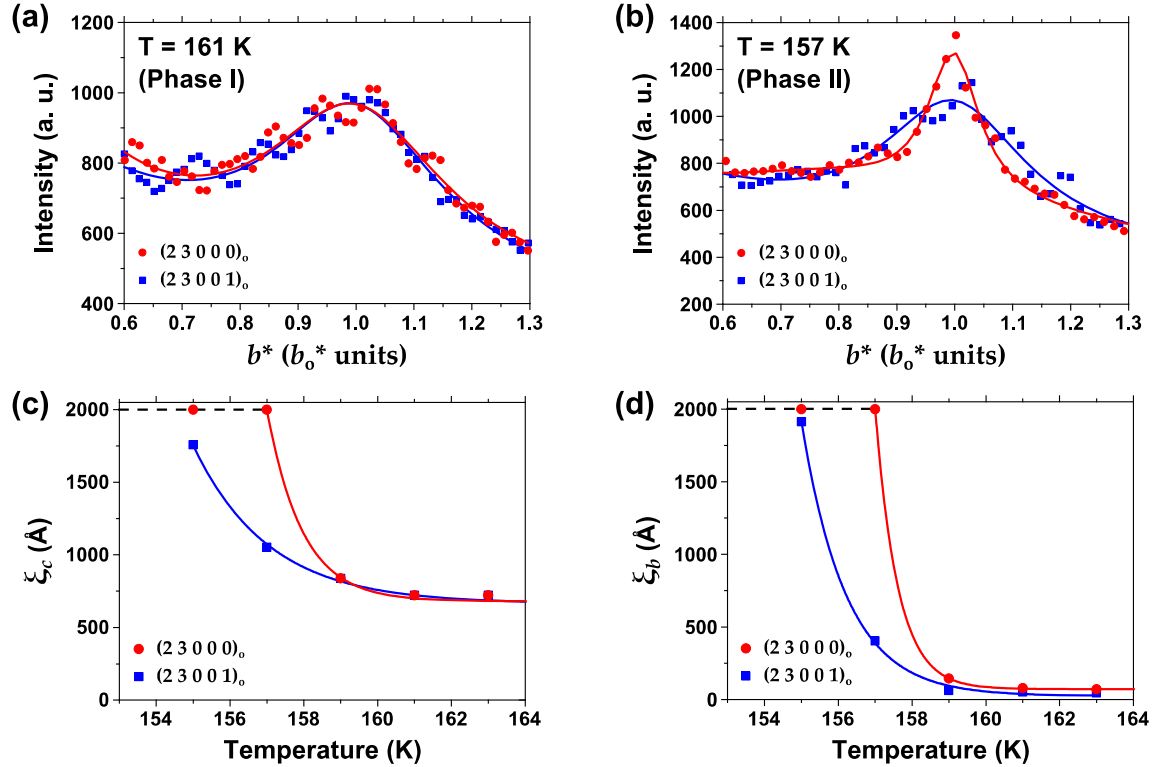

FIG. 9. (Color online) Top: Profiles of (2 3 0 0 0)$_o$ (red circles) and (2 3 0 0 1)$_o$ (blue squares) along b_o* at T = 161 K (a) and T = 157 K (b) for n-octadecane/urea. Bottom: correlation

12

lengths along c_h^* (c) and b_o^* (d) as extracted from the profiles of diffuse scattering for $(2\ 3\ 0\ 0\ 0)_o$ (red circles) and $(2\ 3\ 0\ 0\ 1)_o$ (blue squares). The horizontal dashed lines indicate the resolution limit. The lines are guides for the eyes. All measurements were performed using $15°\ \phi$ rotations at a detector distance of 300 mm on beamline 14-BM-C at the APS. We note here that T_{c2} for *n*-octadecane/urea is ~1.8 K higher than in *n*-octadecane/urea-d4.

Figure 9 shows that in *n*-octadecane/urea, the scattering intensity at q_{c2}, while present in Phase I at 161 K and throughout Phase II, does not turn into sharp Bragg peaks until the sample is cooled to T_{c2} = 154.5 K. This illustrates that the supplementary modulation is present during Phase II, but has only short-range order. Thus, the maximum orthorhombic space group of Phase II has rank four and is $P2_12_12_1(00\gamma)$. This feature is similar to the one reported in solid C_{60}, going from its high-symmetry, face-centered, cubic phase to the simple cubic one [3-5]. It corresponds here to conflicting ordering parameters within the crystal. One of these, which condenses at q_{c1}, corresponds to additional ordering of the guest along b_o, as exhibited by a transition to an orthorhombic basis and a doubling of the unit cell volume. The other one, which emerges as long-range order only below T_{c2}, corresponds to fluctuating excitations associated with an increase of the dimension of the superspace from four to five. The ordering along b_o that was present in Phase II is replaced by the long-range supplementary modulation along c at T_{c2}.

In Phase III, the the peaks satisfying the condition $h + k + n$ = odd are systematically absent, with the $(1\ 2\ 0\ 0\ 0)_o$ common superstructure Bragg peak clearly seen to decrease in intensity below T_{c2} in Fig. 7. The maximum orthorhombic space group is rank five with superspace group $C222_1(00\gamma)(10\delta)$. This C-centered phase presents the same crystallographic signature previously reported in crystals of *n*-nonadecane/urea and *n*-tetracosane/urea [19, 32]. The transition from Phase II to Phase III is associated with the divergence of the correlation lengths measured around q_{c2} at position $(0\ 1\ 0\ 0\ 1)_o$ using the five-dimensional basis and concerns a doubling only of the internal space of the five-dimensional superspace. The systematic absences related to C-centering in Phase III are due to a shift of the supplementary modulation by $c_m/2$ along c (a 180º phase change) between adjacent channels along b_o [6, 18, 19, 32].

Phase IV is similar to Phase II, but with an important difference: in Phase II the supplementary modulation had only short-range order, but in Phase IV, all of the diffraction peaks in the superstructure lines are Bragg peaks, a sign of long-range order for the supplementary modulation. A rank five superspace group is then required to describe this

phase, as in Phase III. Figures 7 and 10 show that Phase IV is marked by the presence of strong common and $h + k + n$ = odd guest Bragg peaks that are absent in Phase III. Systematic absences of h odd in (h 0 0 0 0) and k odd in (0 k 0 0 0) in Phase IV support the presence of 2_1 screw axes along both a and b and implies orthorhombic Laue symmetry. Because the helical structure of the host is incompatible with a twofold axis along c [11], this rules out space group $P2_12_12$, and the five-dimensional superspace group for Phase IV is therefore $P2_12_12_1(00\gamma)(00\delta)$. Upon cooling below T_{c3}, the transition from a C-centered to a primitive cell indicates that there is no longer a phase shift of $c_m/2$ between the supplementary modulations in neighboring channels along b_o and that the interchannel guest ordering present in Phase II is reinstated. This transition is similar to that previously reported in n-nonadecane/urea [18, 19] and n-tetracosane/urea [32].
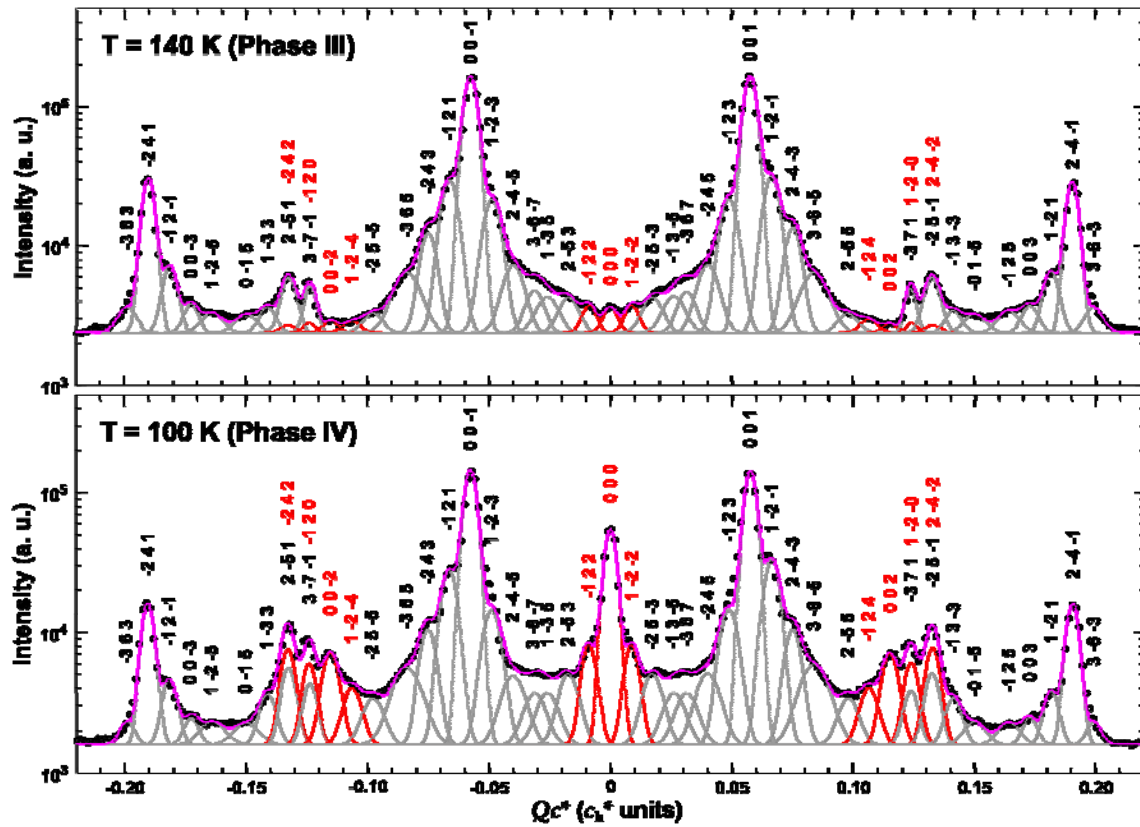

FIG. 10. (Color online) Central section of the (1 2 l m n)$_o$ layer line along c_h* of n-octadecane/urea in Phase III at 140 K (top) and in Phase IV at 100 K (bottom). The data (black circles) are modeled using a sum of Gaussian peaks whose l, m, and n indices are shown above each peak. Note that the intensity scale is logarithmic and that the relative intensities of the overlapped peaks around Qc_h* = ±0.13 are unknown. The misfit parameters used were γ = 0.43802 and δ = 0.0576. The n = even peaks (red) are much more intense in

Phase IV and their presence in Phase III is almost certainly due to synchrotron beam damage. Measurements were made using 60° ϕ rotations about the crystal c axis at a detector distance of 800 mm on beamline 14-BM-C at the APS.

The transition from Phase III to Phase IV is observed at $T_{c3} = 109(4)$ K upon cooling (Fig. 7), and at $T_{c3} = 122.3(1)$ K upon heating (Fig. 11). Such hysteresis between the C-centered and primitive space groups is similar to that observed in n-tetracosane/urea [32]. The phase transitions between these different ambient-pressure phases are found to be continuous or weakly discontinuous, which supports group/subgroup symmetry breaking in each case.
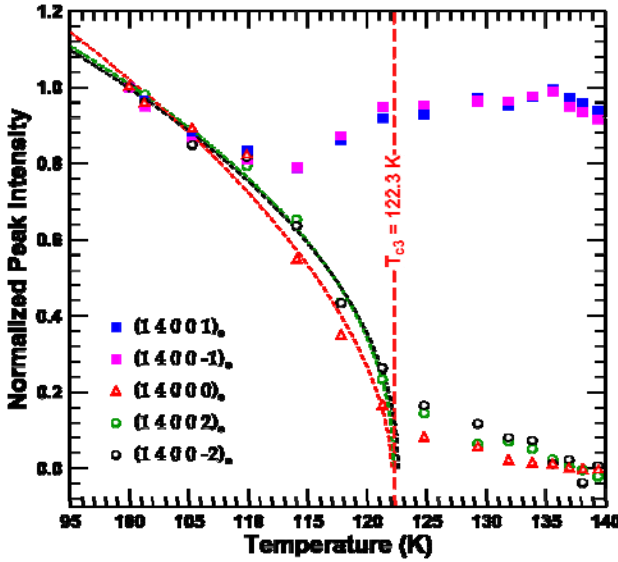

FIG. 11. (Color online) Normalized peak intensities as a function of temperature upon heating as measured from the $(1\ 4\ l\ m\ n)_o$ layer line of n-octadecane/urea. Dashed lines are fits to $A(T_{c3} - T)^\beta$ for the n = even peaks that are present in Phase IV. The critical exponent, β, was measured to be 0.6(1), 0.47(5) and 0.48(8) for $(1\ 4\ 0\ 0\ 0)_o$, and $(1\ 4\ 0\ 0\ 2)_o$, and $(1\ 4\ 0\ 0\ -2)_o$ peaks, respectively. Measurements were made using 60° ϕ rotations about the crystal c axis at a detector distance of 440 mm on beamline 14-BM-C at the APS.

TABLE 1. Sequence of phases for n-octadecane/urea-d_4 and n-octadecane/urea showing the superspace groups, lattice vector bases, and critical wavevectors. The phase transition temperatures at the top correspond to those obtained from X-ray data while cooling n-

octadecane/urea-d_4 with the associated T_c values for unlabeled *n*-octadecane/urea in parentheses (where known).

		$T_{c3} = 109(4)$ K ($T_{c3} = 107$ K)	$T_{c2} = 152.8(4)$ ($T_{c2} = 154.5$ K)	$T_{c1} = 158.1(4)$ K	
Phase	IV		III	II	I
Space Group	$P2_12_12_1(00\gamma)(00\delta)$		$C222_1(00\gamma)(10\delta)$	$P2_12_12_1(00\gamma)$	$P6_122(00\gamma)$
Basis	$(a^*, b^*, c_h^*, c_g^*, c_m^*)_o$		$(a^*, b^*, c_h^*, c_g^*, c_m^*)_o$	$(a^*, b^*, c_h^*, c_g^*)_o$	$(a^*, b^*, c_h^*, c_g^*)_h$
Critical vector	$(0\ 1\ 0\ 0\ 0)_o$		$(0\ 1\ 0\ 0\ 1)_o$	$(0\ 1\ 0\ 0)_o$	$(0\ \tfrac{1}{2}\ 0\ 0)_h$ $(0\ \tfrac{1}{2}\ \delta\ 0)_h$

V. CONCLUSIONS

The aperiodic composite of *n*-octadecane/urea provides a rich sequence of phases in which frustrated interactions compete within higher dimensional crystallographic superspaces. Between 200 K and 100 K, this system undergoes three distinct phase transitions while maintaining the same incommensurate misfit parameter γ. At T_{c1}, the system undergoes a phase transition associated with a very weak C_p anomaly that takes it from a rank four hexagonal system with superspace group $P6_122(00\gamma)$ (Phase I) to an undistorted orthorhombic system, also of rank four, with maximal superspace group $P2_12_12_1(00\gamma)$ (Phase II). This phase transition does not involve any apparent ferroelastic distortion, but the doubling of the unit cell within the ***ab*** plane is demonstrated by the emergence of Bragg peaks in superstructure layer lines with $h+k$ odd, the weakness of which prohibits any structural resolution. This cell doubling might concern either one or both subsystems, as shown by the appearance of the common superstructure Bragg peaks.

The pretransitional fluctuations within the high symmetry phase appear at inequivalent critical points q_{c1} and q_{c2}, but only one of them (q_{c1}) condenses at T_{c1}, in a manner, for example, as previously reported in the 3D crystal of fullerene [3-5]. Unlike fullerene, however, with further cooling, the fluctuations in *n*-octadecane/urea condense at q_{c2} at the expense of the primitive interchannel guest ordering associated with q_{c1}; this is allowed by an increase of the dimensionality of the crystallographic superspace from 4D to 5D. Dynamical

hypotheses involving either phonon or phason softening may explain such frustration and increase in dimensionality [6]. Inelastic neutron or X-ray scattering studies could be used to distinguish these possibilities.

The phase transition at T_{c2} is associated with a large C_p anomaly and a pronounced ferroelastic distortion. The original feature of the transition from Phase II to Phase III is that it takes the crystal from a primitive orthorhombic structure to a C-centered orthorhombic one, as evidenced by the disappearance in Phase III of the common superstructure Bragg peaks. In this transition, the crystal moves from rank four to rank five, as shown by the appearance of satellite Bragg peaks that are closely-spaced along c^* in the superstructure layer lines of Phase III. The wavelength ($c_m = 190(3)$ Å) of the supplementary modulation associated with these new satellites is not an integral multiple of the guest repeat, so the positions of reflections along c^* are now characterized by two independent misfit parameters, γ and δ.

In Phase III, the C-centering arises not from a change in the mean structure, but by a shift in the supplementary modulation by $c_m/2$ along c between adjacent channels along b_o. In this way, Phase III is similar to the C-centered phases reported previously in *n*-nonadecane/urea [18, 19] and *n*-tetracosane/urea [32]. As in these other systems, sixfold non-merohedral twinning and alkane disorder create a formidable challenge to structure solution and refinement. A qualitative interpretation of the physical meaning of the long-range modulations in these C-centered phases is given in Figure 2 of [6].

References

[1]   E. M. Lifshitz and L. P. Pitaevskii, *Physical Kinetics. Course of Theoretical Physics,* Vol. 10, Oxford, 1981).

[2]   P. M. Chaikin and T. C. Lubensky, *Principles of Condensed Matter Physics*, (Cambridge University Press, Cambridge, 1995).

[3]   P. A. Heiney, J. E. Fischer, A. R. McGhie, W. J. Romanow, A. M. Denenstein, J. P. McCauley, Jr., A. B. Smith III, and D. E. Cox, *Phys. Rev. Lett.* **66**, 2911 (1991).

[4]   P. Launois, S. Ravy, and R. Moret, *Phys. Rev. B,* **52**, 5414 (1995).

[5]   S. Ravy, P. Launois, and R. Moret, *Phys. Rev. B* **53**, 10532 (1996).

[6]   C. Mariette, L. Guérin, P. Rabiller, C. Ecolivet, P. García-Orduña, P. Bourges, A. Bosak, D. de Sanctis, M. D. Hollingsworth, T. Janssen, and B. Toudic, *Phys. Rev. B* **87**, 104101 (2013).

[7]   T. Janssen, G. Chapuis, and M. de Boissieu, *Aperiodic Crystals: From Modulated Phases to Quasicrystals* (Oxford University Press, Oxford, 2007).

[8]   T. Janssen, *Acta Crystallogr. A* **68**, 667 (2012).

[9]   P. Coppens, *Acta Crystallogr. B* **51**, 402 (1995).

[10]   S. van Smaalen, *Incommensurate Crystallography* (Oxford University Press, Oxford, 2007).

[11]   C. Mariette, M. Huard, P. Rabiller, S. M. Nichols, C. Ecolivet, T. Janssen, K. E. Alquist III, M. D. Hollingsworth, and B. Toudic, *J. Chem. Phys.* **136**, 104507 (2012).

[12]   M. D. Hollingsworth and K. D. M. Harris, in *Comprehensive Supramolecular Chemistry*, edited by D. D. MacNicol, F. Toda, and R. Bishop (Elsevier Science, Oxford, 1996), p. 177.

[13]   K. D. M. Harris and J. M. Thomas, *J. Chem. Soc., Faraday Trans.* **86**, 2985 (1990).

[14]   S. van Smaalen and K. D. M. Harris, *Proc. R. Soc. London, Ser. A* **452**, 677 (1996).

[15]   R. Lefort, J. Etrillard, B. Toudic, F. Guillaume, T. Breczewski, and P. Bourges, *Phys. Rev. Lett.* **77**, 4027 (1996).

[16]   T. Weber, H. Boysen, F. Frey, and R. B. Neder, *Acta Crystallogr. B* **53**, 544 (1997).

[17]   A. R. George and K. D. M. Harris, *J. Mol. Graphics* **13**, 138 (1995).

[18]   B. Toudic, P. Garcia, C. Odin, P. Rabiller, C. Ecolivet, E. Collet, P. Bourges, G. J. McIntyre, M. D. Hollingsworth, and T. Breczewski, *Science* **319**, 69 (2008).

[19]   B. Toudic, P. Rabiller, L. Bourgeois, M. Huard, C. Ecolivet, G. J. McIntyre, P. Bourges, T. Breczewski, and T. Janssen, *Europhys. Lett.* **93**, 16003 (2011).

[20]   H. U. Lenné, H. C. Mez, and W. Schlenk, Jr., *Justus Liebigs Ann. Chem.* **732**, 70 (1970).

[21]   Y. Chatani, H. Anraku, and Y. Taki, *Mol. Cryst. Liq. Cryst.* **48**, 219 (1978).

[22]   R. Forst, H. Boysen, F. Frey, H. Jagodzinski, and C. Zeyen, *J. Phys. Chem. Solids* **47**, 1089 (1986).

[23]   R. Forst, H. Jagodzinski, H. Boysen, and F. Frey, *Acta Crystallogr. B* **43**, 187 (1987).

[24]   R. Forst, H. Jagodzinski, H. Boysen, and F. Frey, *Acta Crystallogr. B* **46**, 70 (1990).

[25]   K. Fukao, *J. Chem. Phys.* **92**, 6867 (1990).

[26]   K. Fukao, T. Horiuchi, S. Taki, and K. Matsushige, *Mol. Cryst. Liq. Cryst.* **180B**, 405 (1990).

[27]   K. D. M. Harris, I. Gameson, and J. M. Thomas, *J. Chem. Soc., Faraday Trans.* **86**, 3135 (1990).

[28]   A. J. O. Rennie and K. D. M. Harris, *J. Chem. Phys.* **96**, 7117 (1992).

[29]   R. M. Lynden-Bell, *Mol. Phys.* **79**, 313 (1993).

[30]   T. R. Welberry and S. C. Mayo, *J. Appl. Crystallogr.* **29**, 353 (1996).

[31]   T. Weber, H. Boysen, and F. Frey, *Acta Crystallogr. B* **56**, 132 (2000).

[32]   L. Guérin, C. Mariette, P. Rabiller, M. Huard, S. Ravy, P. Fertey, S. M. Nichols, B. Wang, S. C. B. Mannsfeld, T. Weber, M. D. Hollingsworth and B. Toudic, *Phys. Rev. B* **91**, 184101 (2015).

[33]   S. Zerdane, C. Mariette, G. McIntyre, M. H. Lemée-Cailleau, P. Rabiller, L. Guérin, J. C. Ameline, and B. Toudic, *Acta Crystallogr. B* **71**, 293 (2015).

[34]   S. C. B. Mannsfeld, M. L. Tang, and Z. Bao, *Adv. Mater.* **23**, 127 (2011).

[35]   MATLAB Release R2013b, The MathWorks Inc., Natick, Massachusetts, U.S.A.

[36]   A. López-Echarri, I. Ruiz-Larrea, A. Fraile-Rodríguez, J. Díaz-Hernández, T. Breczewski, and F. H. Bocanegra, *J. Phys.: Condens. Matter* **19**, 186221 (2007).